Relativistic GVVPT2 Multireference Perturbation Theory Description of the Electronic States of Y-2 and Tc-2

ARTICLE *in* THE JOURNAL OF PHYSICAL CHEMISTRY A · JANUARY 2014

Impact Factor: 2.69 · DOI: 10.1021/jp409426n · Source: PubMed

4 AUTHORS, INCLUDING:

Patrick K Tamukong
North Dakota State University
3 PUBLICATIONS **10** CITATIONS
SEE PROFILE

Zhendong Li
Peking University
15 PUBLICATIONS **169** CITATIONS
SEE PROFILE

Wenjian Liu
Peking University
98 PUBLICATIONS **2,169** CITATIONS
SEE PROFILE

THE JOURNAL OF PHYSICAL CHEMISTRY A

Article

pubs.acs.org/JPCA

Relativistic GVVPT2 Multireference Perturbation Theory Description of the Electronic States of Y_2 and Tc_2

Patrick K. Tamukong,[†] Mark R. Hoffmann,*[,†] Zhendong Li,[‡] and Wenjian Liu*[,‡]

[†]Chemistry Department, University of North Dakota, Grand Forks, North Dakota 58202, United States.

[‡]Beijing National Laboratory for Molecular Sciences, Institute of Theoretical and Computational Chemistry, State Key Laboratory of Rare Earth Materials Chemistry and Applications, College of Chemistry and Molecular Engineering, and Center for Computational Science and Engineering, Peking University, Beijing 100871, People's Republic of China

Supporting Information

ABSTRACT: The multireference generalized Van Vleck second-order perturbation theory (GVVPT2) method is used to describe full potential energy curves (PECs) of low-lying states of second-row transition metal dimers Y_2 and Tc_2, with scalar relativity included via the spin-free exact two-component (sf-X2C) Hamiltonian. Chemically motivated incomplete model spaces, of the style previously shown to describe complicated first-row transition metal diatoms well, were used and again shown to be effective. The studied states include the previously uncharacterized $2^1\Sigma_g^+$ and $3^1\Sigma_g^+$ PECs of Y_2. These states, together with $1^1\Sigma_g^+$, are relevant to discussion of controversial results in the literature that suggest dissociation asymptotes that violate the noncrossing rule. The ground state of Y_2 was found to be $X^5\Sigma_u^-$ (similar to Sc_2) with bond length R_e = 2.80 Å, binding energy D_e = 3.12 eV, and harmonic frequency ω_e = 287.2 cm^{-1}, whereas the lowest $1^1\Sigma_g^+$ state of Y_2 was found to lie 0.67 eV above the quintet ground state and had spectroscopic constants R_e = 3.21 Å, D_e = 0.91 eV, and ω_e = 140.0 cm^{-1}. Calculations performed on Tc_2 include study of the previously uncharacterized relatively low-lying $1^5\Sigma_g^+$ and $1^9\Sigma_g^+$ states (i.e., 0.70 and 1.84 eV above $1^1\Sigma_g^+$, respectively). The ground state of Tc_2 was found to be $X^3\Sigma_g^-$ with R_e = 2.13 Å, D_e = 3.50 eV, and ω_e = 336.6 cm^{-1} (for the most stable isotope, Tc-98) whereas the lowest $^1\Sigma_g^+$ state, generally accepted to be the ground state symmetry for isovalent Mn_2 and Re_2, was found to lie 0.47 eV above the $X^3\Sigma_g^-$ state of Tc_2. The results broaden the range of demonstrated applicability of the GVVPT2 method.

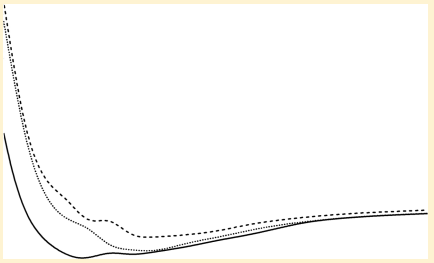

1. INTRODUCTION

Yttrium (Y) and technetium (Tc) appear in the second transition series of the periodic table and exist in states arising from the ^2D ($4d^15s^2$) and ^6S ($4d^55s^2$) ground atomic terms, respectively, although calculations by Klyagina et al.[1] on the spin states of Tc_2 suggested a ^6D ($4d^65s^1$) ground state for the Tc atom. Interest in these elements is due in part to their many important applications; e.g., technetium-99m (the metastable form of isotope Tc-99) is widely used in radiopharmaceuticals as a clinical tracer element for both diagnostic and therapeutic purposes.[2] Some compounds of yttrium also have medical applications; e.g., Y-90 yttrium complexes are used in radioimmunotherapy,[3] and oxides of yttrium are used in television tubes and in ceramics and glasses.[4] Technetium is the lightest radioactive and first artificial element, discovered in 1925 by Noddack et al.,[5] who named it masurium, from the analysis of platinum ores and columbite minerals; it was obtained later by Perrier and Segrè (see refs 6 and 7) from the analysis of molybdenum bombarded by deuterium nuclei. Technetium has 34 known isotopes, all of which are radioactive, with masses in the range [85, 118], the most abundant being Tc-99, which is largely present in spent nuclear fuel and has a half-life of 2.1 × 10^5 years.[8] We considered Tc-98, which has the longest half-life of any isotope (4.2 million years), in the present calculations.

Previous experimental and theoretical studies of the yttrium dimer (Y_2) have been inconclusive. Just like its isovalent counterpart, Sc_2, Y_2 appears simple with only 6 valence electrons but is quite challenging; e.g., the true symmetry of its ground state is unresolved. Contradictory results for the ground state of Sc_2 are between $^5\Sigma_u^-$ and $^3\Sigma_u^-$; for Y_2, they are between $^5\Sigma_u^-$ and $^1\Sigma_g^+$. Experimentally, the binding energy of the supposed ground state of Y_2 was determined by Verhaegen et al.[9] as 1.62 ± 0.22 eV, using the third law method, but this method is unreliable due to inherent limitations resulting from the requirement of knowledge of the unknown electronic structure. Knight et al.[10] observed the electron spin resonance (ESR) spectra of Y_3 in a matrix isolation technique but failed to obtain the same for Y_2. Yang et al.[11] determined the Y_2 ground state as $^5\Sigma_u^-$ with a harmonic frequency, ω_e = 185 ± 0.2 cm^{-1} in a pulsed-field-ionization zero-kinetic-energy (PFI-ZEKE) photoelectron spectroscopic study. Fang et al.[12] obtained ω_e = 184.4 ± 0.4 cm^{-1} and D_e = 3.5 ± 0.4 eV in a mass-selected resonance Raman matrix isolation study of Y_2 and computed R_e = 2.65 Å using Badger's rule. These authors assigned the ground state of Y_2 as $^1\Sigma_g^+$. The ground state symmetry obtained from the gas phase study of Yang et al.[11] is

Received: September 21, 2013
Revised: January 28, 2014
Published: January 30, 2014

dx.doi.org/10.1021/jp409426n | J. Phys. Chem. A 2014, 118, 1489−1501

Table 1. Equilibrium Distances (R_e), Binding Energies (D_e), Adiabatic Transition Energies (T_e), and Harmonic Frequencies (ω_e) of Electronic States of Y_2 Calculated at the sf-X2C GVVPT2 Level Compared with Results from Other Methods

method	basis set	R_e (Å)	D_e (eV)	ω_e (cm^{-1})	T_e (eV)
		$X^5\Sigma_u^-$			
CASSCF-CI[a]		3.03	2.44	171.0	
CASSCF/SOCI+Q[b]	RECP	3.03	2.60	172.0	
DFT(VWN-BP)[c]	slater-type triple ζ	2.94		173.0	
DFT(B3P86)[c]	LANL2DZ	2.73		214.0	
DFT(BOP)[d]	(23s18p15d4f/9s5p6d2f)	2.96	2.14	173.3	
DFT(B3LYP)[e]	CEP-121G	2.76	0.22	204.4	
DFT(BLYP)[e]	CEP-121G	2.79	0.56	193.5	
DFT(B3PW91)[e]	CEP-121G	2.75	0.68	206.9	
DFT(BHLYP)[e]	CEP-121G	2.74	0.47	213.9	
DFT(BP86)[e]	CEP-121G	2.76	1.03	198.7	
DFT(B3P86)[e]	CEP-121G	2.73	0.72	208.9	
DFT(SVWN)[e]	CEP-121G	2.72	1.73	206.8	
DFT(mPW1PW91)[e]	CEP-121G	2.74	0.64	208.8	
DFT(PBE1PBE)[e]	CEP-121G	2.74	0.66	209.2	
GVVPT2	aug-cc-pVTZ-DK	2.80	3.12	287.2	
experiment			1.62 ± 0.22[f]	185 ± 0.2[c]	
		2.65[g]	3.5 ± 0.4[g]	184.4 ± 0.4[g]	
		$1^1\Sigma_g^+$			
CASSCF-CI[a]		2.74	2.93[h]	206.0	0.87
CASSCF/SOCI+Q[b]	RECP	2.76	3.09[h] (0.37)[i]	180.0	0.87
DFT(VWN-BP)[c]	slater-type triple ζ	2.59		207.0	0.29
DFT(B3P86)[c]	LANL2DZ	2.76		225.0	0.96
GVVPT2	aug-cc-pVTZ-DK	3.21	0.91	140.0	0.67
		$2^1\Sigma_g^+$			
GVVPT2	aug-cc-pVTZ-DK	3.27	0.75	122.9	0.83
		$3^1\Sigma_g^+$			
GVVPT2	aug-cc-pVTZ-DK	3.36 (4.27)	0.09 (0.10)	118.3 (113.9)	1.49 (1.48)

[a]Reference 13. [b]Reference 15. [c]Reference 11. [d]Reference16. [e]Reference 17. [f]Reference 9 (third law method). [g]Reference 12 (reported a $^1\Sigma_g^+$ ground state). [h]Dissociation to excited state atoms (Y: $4d^25s^1$). [i]Dissociation to ground state atoms (Y: $4d^15s^2$).

probably the more reliable one, as matrices can affect the relative stabilities of electronic states of trapped molecules.

Theoretical results on Y_2 in the literature are not less contradictory. Walch and Bauschlicher,[13] using the complete active space self-consistent field configuration interaction approach (CASSCF-CI), found the ground state of Y_2 to be $^5\Sigma_u^-$ (with a dominant configuration similar to that for the $^5\Sigma_u^-$ ground state of Sc_2) with the $^1\Sigma_g^+$ state of Y_2 lying 0.87 eV above the $^5\Sigma_u^-$ state in the vicinity of the equilibrium bond length. Data from these studies are shown in Table 1. However, these authors found the lowest $^1\Sigma_g^+$ state to have a major configuration that results from two excited state Y atoms with configuration $5s^14d^2$. This warrants further consideration because a $^1\Sigma_g^+$ state can also result from the coupling of two doublet ground state Y atoms ($5s^24d^1$: ^2D_g) and is expected to lie lower in energy. The PEC of Walch and Bauschlicher for the lowest $^1\Sigma_g^+$ state of Y_2 therefore violates the noncrossing rule. In fact, because Y_2 is isovalent with Sc_2, following the analysis of Kalemos et al.[14] on the molecular states of Sc_2, the combination of two doublet ground state atoms of Y should result in a total of 30 molecular terms, 3 of which are of $^1\Sigma_g^+$ symmetry. The noncrossing rule therefore implies that the first three lowest $^1\Sigma_g^+$ states should correlate with the $5s^24d^1 + 5s^24d^1$ dissociation asymptote. This is indeed what we observed in the present work, as will be seen below. Balasubramanian and Dai[15] employed second-order CI with Davidson correction for unlinked quadruple clusters (SOCI + Q) following a CASSCF reference wave function, in which the $4s^24p^64d^15s^2$ shells were included in the valence space, with a relativistic effective core potential (RECP) basis set, and obtained a $^5\Sigma_u^-$ ground state. These authors also found the lowest $^1\Sigma_g^+$ state to be 0.87 eV less stable than the $X^5\Sigma_u^-$state at the CASSCF/SOCI + Q level and 0.55 eV less stable at the MRSDCI level of theory (cf. Table 1).

Previous DFT results on the Y_2 molecule have tended to favor a quintet ground state. Yang et al.[11] obtained a $^5\Sigma_u^-$ ground state for Y_2 at the DFT level using the Vosko–Wilk–Nussair parametrization of the local density approximation augmented with Becke's generalized gradient approximation to the exchange energy and Perdew's expression for the correlation energy. These authors found the $1^1\Sigma_g^+$ state of Y_2 to lie 0.29 eV above the quintet ground state with the same leading equilibrium-geometry configuration as reported in the Walch and Bauschlicher ab initio study.[13] Data from these studies plus those from other DFT calculations,[16,17] e.g., using the hybrid B3P86 functional which combines the Becke three-parameter exchange functional with the Perdew correlation functional and using a LANL2DZ basis set, are included in Table 1.

Information on Tc_2 is quite sparse in the literature. Much more is known about Tc derivatives that are useful primarily in radiopharmaceuticals and corrosion protection. Many complexes with a Tc_2 nucleus have been reported in the literature, e.g., $Tc_2(O_2CC(CH_3)_3)_4Cl_2$ with a Tc–Tc bond length of 2.19 Å,[18] $Tc_2Cl_8^{3-}$ with a Tc–Tc bond length of 2.12 Å,[19] and α- and β-$TcCl_3$, which are polymorphs of triangular Tc_3Cl_9 units

Table 2. Equilibrium Distances (R_e), Binding Energies (D_e), Adiabatic Transition Energies (T_e), and Harmonic Frequencies (ω_e) of Electronic States of Tc_2 Calculated Using Spin-Free X2C Relativistic GVVPT2 Compared with Results from Other Methods and from Experiment

method	basis set	R_e (Å)	D_e (eV)	ω_e (cm^{-1})	T_e (eV)
		$X^3\Sigma_g^-$			
DV-X_α[a]		1.92			
DFT (BOP)[b]	(23s18p15d4f/9s5p6d2f)	1.97	4.75	512.0	
DFT (B3LYP)[b]	(23s18p15d4f/9s5p6d2f)	1.93	3.15	557.6	
DFT(B88)[b]	(23s18p15d4f/9s5p6d2f)	1.99	1.46	483.5	
MP2[b]	(23s18p15d4f/9s5p6d2f)	unbound[c]	unbound	unbound	
DFT[d]	slater-type triple ζ	2.01			
CASSCF/CASPT2[e]	ANO-RCC VTZP	1.94	3.30[f]	492.0	
GVVPT2	aug-cc-pVTZ-DK	2.13	3.50	336.6	
experiment[i]			3.49,[g] 3.45,[g] 3.33,[g] 2.93[h]		
		$1^{11}\Sigma_g^-$			
DFT (B3LYP)[j]		2.84	2.27	178.5	
GVVPT2	aug-cc-pVTZ-DK	2.47	1.13	225.1	2.38
		$1^1\Sigma_g^+$			
CASSCF/CASPT2[e]	ANO-RCC-VTZP	1.97		450.0	0.22
GVVPT2	cc-pVTZ-DK	2.21	2.82	244.1	
GVVPT2	aug-cc-pVTZ-DK	2.19	3.18	253.9	0.47
		$1^5\Sigma_g^+$			
GVVPT2	aug-cc-pVTZ-DK	2.31	2.49	246.9	0.70
		$1^9\Sigma_g^+$			
GVVPT2	aug-cc-pVTZ-DK	2.69	1.35	235.0	1.84

[a]Reference 28 and 29. [b]Reference 16. [c]This method rather predicted a ground $^7\Pi_u$ state with R_e = 2.18 Å, D_e = 3.97 eV and ω_e = 349.3 cm^{-1}. [d]Reference 30. [e]Reference 24. [f]After considering spin−orbit coupling effects; [g]Reference 27. [h]Reference 28 and 29. [i]Values computed from thermodynamic relations using dissociation, vaporization and metal surface enthalpies. [j]Reference 31.

with Tc−Tc bond lengths of 2.44 and 2.86 Å, respectively.[20,21] These complexes all showed evidence of multiple d−d bonding in the Tc_2 moiety. This is contrary to isovalent Mn, which is not known to form compounds with ligated Mn_2 species.[22] Metal−metal bonding in transition metals can be understood in terms of two factors: the relative sizes of the $(n-1)$d and ns orbitals and the $ns \rightarrow (n-1)$d excitation energy. For group VIIB metals, the relative sizes of the $(n-1)$d and ns orbitals become similar in spatial extent on going from Mn to Re (probably due to relativistic effects tending to contract the outer ns and slightly expand the inner $(n-1)$d orbitals) such that, for ground state atoms, the ratio $(\langle r_{(n+1)s}\rangle/\langle r_{nd}\rangle)$ is 2.99 for Mn, 2.27 for Tc, and 2.11 for Re.[13] The $ns \rightarrow (n-1)$d excitation energy decreases from Mn to Tc (i.e., Mn = 2.14 eV; Tc = 0.41 eV) but increases again from Tc to Re (1.76 eV).[23] This decrease favors s−d hybridization, and hence d−d bonds. Mn_2 can be understood to be a van der Waals species due to the high s−d promotion energy and differences in the spatial extents of the 3d and 4s orbitals, whereas multiple bonds have been reported in the Tc_2 and Re_2 molecules.[24] Consequently, calculations comparing Mn_2 and Tc_2 provide insight into relativistic effects.

Because all 34 known isotopes of Tc are radioactive, little experimental work has been carried out on this element and has been limited to spectroscopic studies on the atom (e.g., see ref 25 and references therein). We did not find experimental data on Tc_2 in the literature apart from values of the binding energy of the supposed ground term of Tc_2 computed from thermodynamic relations by Miedema and Gingerich[26] and by Brewer and Winn.[27] On the basis of three different expressions relating the dissociation enthalpy to the enthalpy of vaporization and the metal surface enthalpy, Miedema and Gingerich[26] computed D_0 values of 3.49, 3.45, and 3.33 eV for Tc_2. Brewer and Winn[27] computed D_0 = 2.93 eV for ground state Tc_2 (i.e., 0.40 eV less than the lowest value obtained be Miedema and Gingerich[26]).

The Tc_2 molecule is better known theoretically than experimentally. Klyagina et al.[28,29] obtained R_e = 1.92 Å for Tc_2 using the discrete variational X_α (DV-X_α) method. Yanagisawa et al.[16] studied second-row transition metal (TM) dimers at the DFT level, employing different functionals, and also at the MP2 level (Table 2). They found the ground state of Tc_2 to be $^3\Sigma_g^-$ with R_e = 1.93 Å, and ω_e = 557.6 cm^{-1} with the B3LYP hybrid functional with the same major configuration around the minimum as was observed by Klyagina et al.[28,29] Most DFT functionals used by them and others[30] gave comparable equilibrium bonds lengths, but binding energies that varied by over 3 eV. In contrast, the MP2 calculations by Yanagisawa et al.[16] found the $^3\Sigma_g^-$ state to be unbound and instead predicted a ground $^7\Pi_u$ state around the minimum, suggesting a triple bond. Even more exotic, Yan and Zhu[31] optimized the structure of Tc_2 with the B3P86 functional and found the ground state to be $^{11}\Sigma_g^-$. It appears that the most recent calculations on Tc_2 are due to Borin et al.[24] By applying CASPT2 on a CASSCF reference wave function and accounting for scalar relativity via the Douglas−Kroll−Hess (DKH) Hamiltonian[32−34] and using a quadruple-ζ atomic ANO-RCC basis set,[35] these authors obtained a $^3\Sigma_g^-$ ground state for the Tc_2 molecule with R_e = 1.94 Å and ω_e = 492.0 cm^{-1}, and with an effective bond order (EBO) of 4.4 (interpretable as a pentuple bond). The same authors found the lowest excited Tc_2 state to be $1^1\Gamma_g$ (lying at 1285 cm^{-1} or 0.16 eV above the ground state) with R_e = 1.96 Å and ω_e = 458.0 cm^{-1} and with a configuration similar to that for the ground state and an EBO of 4.3. The lowest $^1\Sigma_g^+$ state, which is the reported ground state symmetry for isovalent Mn_2 and Re_2, was found to lie at some 1797 cm^{-1} or 0.22 eV above

dx.doi.org/10.1021/jp409426n | J. Phys. Chem. A 2014, 118, 1489−1501

Table 3. Performance of Various Approximations to the X and R Matrices for At_2 at R = 2.8373 Å[a]

basis set	full/E_h	error(DLXR)/mE_h		error(DLU)/mE_h	
uncontracted	−45749.06309	−0.0901	(−0.0554)[b]	−0.5601	(−0.0531)[c]
X2C-ANO-LARGE	−45749.06309	−0.0883	(−0.0512)[b]	−0.5580	(−0.0488)[c]
DKH2-ANO-RCC-LARGE	−45746.15276	0.0342	(0.1195)[b]	−0.4344	(0.1233)[c]
X2C-ANO-VTZP	−45749.06050	0.4213	(−0.0538)[b]	−0.0249	(−0.0515)[c]
DKH2-ANO-RCC-VTZP	−45746.14951	0.4526	(0.1086)[b]	0.0001	(0.1123)[c]

[a]Deviations from the Hartree−Fock results with the full one-electron **X** and the full **R** (second column) are shown. DKH2-ANO-RCC: atomic natural orbitals optimized for several electronic states of At at the DKH2-CASPT2 level. X2C-ANO: contracted in the same pattern as DKH2-ANO but based on spin-free X2C Hartree−Fock calculation of single averaged atomic configuration. Contraction patterns: LARGE, [25s22p16d12f4g]/(11s10p9d6f4g); VTZP, [25s22p16d12f4g]/(8s7p5d3f2g). [b]Difference between FATM and DLXR. [c]Difference between ATOMU and DLU.

the Tc_2 ground state and had an EBO of 4.3, and spectroscopic constants essentially identical to the $^3\Sigma_g^-$ ground state. After the inclusion of spin−orbit coupling, these authors observed a strong interaction between the $^3\Sigma_g^-$ and $^1\Sigma_g^+$ states that led to a 0_g^+ ground state with composition = $(0.75)^3\Sigma_g^- + (0.25)^1\Sigma_g^+$ and with R_e = 1.94 Å, D_e = 3.30 eV, and ω_e = 490.0 cm^{-1}.

In this paper, the GVVPT2 method,[36,37] which was recently shown[38] to be capable of describing complicated dimers of first-row TM elements, is shown to be able to describe second-row TM dimers (i.e., Y_2 and Tc_2) with scalar relativity accounted for through the spin-free exact two-component (sf-X2C) Hamiltonian.[39−44] Note that, in contrast to previous work and exploiting GVVPT2's capabilities to describe ground and excited states at arbitrary geometries, full PECs will be reported. In this study, we also performed calculations on the $X^1\Sigma_g^+$ term of Mn_2 with and without relativistic effects included to better understand the isovalent Tc_2 molecule. The rest of the paper is organized as follows. Section 2 briefly reviews the salient features of the sf-X2C Hamiltonian and GVVPT2 method and also describes details as to how the calculations were done, the results are presented and discussed in section 3, and a final section concludes the paper.

2. METHODS

2.1. Spin-Free Exact Two-Component (sf-X2C) Hamiltonian. To describe scalar relativistic effects accurately, we here adopt the following Hamiltonian

$$H = \sum_{pq} [\mathbf{h}_{+,sf}^{X2C}]_{pq} a_p^+ a_q + \frac{1}{2} \sum_{pqrs} (pr|qs) a_p^+ a_q^+ a_s a_r \tag{1}$$

where the one-electron term is the spin-free (sf) part of the exact two-component (X2C) Hamiltonian,[39] whereas the two-electron term is simply the bare Coulomb interaction. The latter is justified by the fact that the so-called scalar relativistic two-electron picture change errors are negligibly small for valence properties.[40,41] The spin−orbit coupling effects are certainly important but which will be considered in future via a molecular mean-field spin−orbit operator.[41,42] The sf-X2C Hamiltonian $\mathbf{h}_{+,sf}^{X2C}$ is constructed here in one step by diagonalizing the spin-free one-electron Dirac equation

$$\mathbf{h}_{sf}^{D}\mathbf{C} = \begin{pmatrix} \mathbf{V} & \mathbf{T} \\ \mathbf{T} & \frac{\alpha^2}{4}\mathbf{W}_{sf} - \mathbf{T} \end{pmatrix} \begin{pmatrix} \mathbf{A} \\ \mathbf{B} \end{pmatrix} = \begin{pmatrix} \mathbf{S} & 0 \\ 0 & \frac{\alpha^2}{2}\mathbf{T} \end{pmatrix} \begin{pmatrix} \mathbf{A} \\ \mathbf{B} \end{pmatrix} E \tag{2}$$

where α is the fine-structure constant, **S**, **T**, and $\mathbf{V}_{ne}$ are the respective matrices of the nonrelativistic metric, kinetic energy and nuclear attraction, and $\mathbf{W}_{sf}$ is the matrix of the operator $W_{sf} = (\vec{p}\cdot V_{ne}\vec{p})$. By virtue of the **X** matrix, i.e., the ratio between the small and large component coefficients of positive energy states,

$$\mathbf{X} = \mathbf{B}_+\mathbf{A}_+^{-1} \tag{3}$$

the $\mathbf{h}_{+,sf}^{X2C}$ Hamiltonian can be constructed as[39]

$$\mathbf{h}_{+,sf}^{X2C} = \mathbf{R}_+^\dagger \mathbf{L}_{+,sf}^{NESC} \mathbf{R}_+ \tag{4}$$

$$\mathbf{L}_{+,sf}^{NESC} = \mathbf{V}_{ne} + \mathbf{TX} + \mathbf{X}^\dagger\mathbf{T} + \mathbf{X}^\dagger\left[\frac{\alpha^2}{4}\mathbf{W}_{sf} - \mathbf{T}\right]\mathbf{X} \tag{5}$$

Although the normalized elimination of the small component (NESC)[43] Hamiltonian, $\mathbf{L}_{+,sf}^{NESC}$, still stays in the Dirac picture (i.e., $\mathbf{L}_+^{NESC}\mathbf{A}_+ = (\tilde{S}_+\mathbf{A}_+E)$ with the relativistic metric $\tilde{S}_+ = (S + (\alpha^2/4)\mathbf{X}^\dagger\mathbf{T}\mathbf{X})$), the $\mathbf{h}_{+,sf}^{X2C}$ Hamiltonian is now in the Schrödinger picture (i.e., $\mathbf{h}_{+,sf}^{X2C}\mathbf{C}_+ = \mathbf{S}\mathbf{C}_+E$ with the nonrelativistic metric **S**) thanks to the picture-change transformation **R**[44]

$$\mathbf{R} = (\mathbf{S}^{-1}\tilde{\mathbf{S}}_+)^{-1/2} = \mathbf{S}^{-1/2}(\mathbf{S}^{-1/2}\tilde{\mathbf{S}}_+\mathbf{S}^{-1/2})^{-1/2}\mathbf{S}^{1/2} \tag{6}$$

The so-obtained Hamiltonian $\mathbf{h}_{+,sf}^{X2C}$ is correct to infinite order in one-electron scalar relativistic effects. It is obviously superior to the widely used approximate Hamiltonians.[32−34]

We take the opportunity to point out that accurate approximations, not invoked here though, can be made for constructing $\mathbf{h}_{+,sf}^{X2C}$ based on the local nature of relativity. For instance, the molecular **X** can simply be approximated by the direct sum of the atomic **X** matrices (denoted as ATOMX) in the spirit of "from atoms to molecule" (FATM).[45,46] In this approach, each atomic matrix is obtained by diagonalizing the atomic one-electron Dirac equation. Alternatively, the **X** matrix can be obtained by solving the one-electron Dirac equation that is block-diagonal in atoms but with all the nuclear attractions accounted for. The so-constructed **X** is to be termed "diagonal local X" (DLX). Similarly, a "diagonal local R" (DLR; block-diagonal in atoms) approximation can be made to the **R** matrix. The combination of DLX and DLR is just the "diagonal local unitary transformation" (DLU) approach proposed recently by Peng and Reiher,[47] whereas the combination of the ATOMX with the full **R** corresponds to the original FATM.[45,46] The combination of the ATOMX with DLR and the combination of DLX and the full **R** may likewise be termed ATOMU and DLXR, respectively. DLU was claimed to be extremely accurate.[47] As can be seen from Table 3, this is indeed the case when DLU is combined with a heavily contracted basis set, e.g., the DKH2-ANO-RCC-VTZP set.[48] However, the accuracy of DLU is greatly deteriorated when less contracted or even uncontracted basis sets are used. Therefore, the claimed accuracy

dx.doi.org/10.1021/jp409426n | J. Phys. Chem. A 2014, 118, 1489−1501

Table 4. Performance of Various Approximations to the X and R Matrices for At_2 at Various Interatomic Distances[a]

R/Å	full/E_h	error(DLXR)/mE_h		error(DLU)/mE_h		ratio	
2.5707	−45749.04285	−0.2091	$(-0.0505)^b$	−1.2857	$(-0.0460)^c$	6.15	$(5.13)^d$
2.6707	−45749.05615	−0.1537	$(-0.0508)^b$	−0.9512	$(-0.0472)^c$	6.19	$(4.88)^d$
2.7707	−45749.06211	−0.1110	$(-0.0510)^b$	−0.6944	$(-0.0482)^c$	6.25	$(4.58)^d$
2.8207	−45749.06303	−0.0936	$(-0.0511)^b$	−0.5897	$(-0.0486)^c$	6.30	$(4.41)^d$
2.8707	−45749.06287	−0.0785	$(-0.0511)^b$	−0.4985	$(-0.0490)^c$	6.35	$(4.22)^d$
2.9207	−45749.06181	−00654	$(-0.0512)^b$	−0.4195	$(-0.0494)^c$	6.41	$(4.02)^d$
2.9707	−45749.06000	−0.0542	$(-0.0513)^b$	−0.3515	$(-0.0497)^c$	6.48	$(3.80)^d$
			Spectroscopic Data				
R_e/Å	2.8373	−0.0008	$(0.0000)^b$	−0.0046	$(0.0000)^c$	6.07	$(6.07)^d$
ω_e/cm^{-1}	169.01	0.05	$(0.00)^b$	0.32	$(0.00)^c$	6.48	$(6.48)^d$

[a]Hartree−Fock calculations with the X2C-ANO-LARGE basis set. Deviations from the results with the full one-electron **X** and the full **R** (second column) are shown. Ratio: Error(DLU)/Error(DLXR). [b]Difference between FATM and DLXR. [c]Difference between ATOMU and DLU. [d]Error(ATOMU)/error(FATM).

of DLU[47] must be regarded as fortuitous. By comparing ATOMU with DLU and FATM with DLXR, one sees that, regardless of the approximate or full **R** matrix, the difference between ATOMX and DLX is merely 0.05 mE_h for either uncontracted or contracted basis sets according to the X2C calculations (i.e., X2C-ANO-LARGE and X2C-ANO-VTZP). The same difference holds across the potential energy curve of At_2 (cf. Table 4) and hence does not affect the equilibrium bond distance and harmonic vibrational frequency. In contrast, the errors of DLU (ATOMU) are 6 (4) times larger than those of DLXR (FATM) and eventually affect the molecular spectroscopic constants. These results clearly reveal that the **R** matrix is somewhat more delocalized than **X**. Similar findings are also observed at the MP2 level, not documented though. Because both the construction of the **R** matrix itself and its use in transforming the one-electron integrals are computationally very cheap, any approximation to **R** should not be recommended. That is, it is the combination of the ATOMX and the full **R** matrix (i.e., FATM) that should be used for large molecules. Finally, it deserves to be pointed out that, though the one-electron approximation to **X** turns out to be very accurate for electronic structure calculations, it breaks down for nuclear magnetic resonance shielding constants.[49] In contrast, the ATOMX constructed by solving the full Dirac equation for each spherical, unpolarized atomic configuration still remains very accurate.

2.2. GVVPT2 Method. Here, we briefly describe only features of GVVPT2 considered salient to the present study because the GVVPT2 method has been thoroughly described elsewhere[36,37,50] (also see refs 38 and 51−53 for recent chemical studies). In the GVVPT2 scheme, we divide the total Hilbert space into a model space, L_M (generally of an MCSCF type), and an external space (L_Q) whose configurations are related to the model space configuration state functions (CSFs) by single and double electron excitations. The GVVPT2 method supports both complete and incomplete model spaces, a capability that was extensively used in this study. The model space is further partitioned into a primary space (L_P), spanned by a set of reference functions (typically the lowest MCSCF states), and its orthogonal complement, called the secondary space (L_S), which constitutes a "buffer zone" between the primary and external spaces. Only states in the primary subspace are perturbatively corrected, but states in both the primary and secondary subspaces are considered in the final diagonalization of the effective Hamiltonian in the total model space. The buffer zone energetically separates the primary and external spaces sufficiently for primary−external (P−Q) interactions to be described perturbatively. This approach circumvents most intruder state problems. Note that the intruder state problems of CASPT2 and MSQDPT were detailed in ref 54 for Mn_2. In the GVVPT2 method, we use nonlinear denominator shifts that vary continuously with excitation energy. This obviates the intruder state problem completely and guarantees smooth continuous PECs for both ground and excited electronic states, even for cases with multiple, and geometry dependent, quasidegeneracies, as is typical of TM systems. To realize this, we incorporate a resolvent that is both degeneracy-corrected and contains a hyperbolic tangent function as a switching function from nondegenerate to degenerate regimes.[36] The choice of $\tanh(x)$ as a switching function satisfies strict mathematical conditions throughout the domain.[36] Also, the GVVPT2 method is inherently spin-adapted, thereby avoiding the spin contamination problem. Because of the capability of including large numbers of one-electron states (i.e., orbitals) with which to construct the model space, rigorous maintenance of a total spin quantum number, and continuity through regions of variable quasidegeneracy, GVVPT2 is well suited to the studies at hand.

2.3. Computational Details. Macroconfigurations[55] were used within the GVVPT2 method in all calculations. In the macroconfiguration approach, the active orbitals are partitioned into groups, which allows for physical intuition, and restrictions are imposed on group occupancies. Each unique assignment of electrons to active orbital groups constitutes one macroconfiguration (denoted MCRM). Within each orbital group, all possible electronic configurations (that combine with those of other orbital groups to give the desired molecular point group symmetry) are allowed. Each MCRM generates a unique set of configurations that is disjoint with the configuration sets of other MCRMs. Finally, CSFs with target spin eigenfunctions are generated from electron configurations. Hamiltonian matrix elements are computed using graphical unitary group approach (GUGA) based algorithms in the undmol electronic structure software package (N.B. undmol is described in detail in ref 56 and is available on request from Prof. Mark Hoffmann at the University of North Dakota). All components of the undmol package are able to make use of Abelian point group symmetry, and additional specialized angular momentum based routines ensured $D_{\infty h}$ symmetry. It can also be noted that the macroconfiguration approach permits a large number of noninteracting electronic configuration pairs to be screened

and, moreover, provides an efficient way of regenerating excited configurations.

The active spaces for Y_2 and Tc_2 consisted of 4d- and 5s-dominated molecular orbitals (MOs) (and in a few cases, $5p_z$-derived MOs) that were partitioned into groups and used to generate reference MCRMs as described below.

For the $^1\Sigma_g^+$, $^5\Sigma_g^+$, and $^9\Sigma_g^+$ states of Tc_2, a single reference MCRM was constructed using five orbital groups; each group had a bonding and a corresponding antibonding MO (superscripts denote occupation numbers).

$$(4d_{xz}\pi_u 4d_{xz}\pi_g^*)^2(4d_{yz}\pi_u 4d_{yz}\pi_g^*)^2(4d_{x^2-y^2}\delta_g 4d_{x^2-y^2}\delta_u^*)^2(4d_{xy}\delta_g 4d_{xy}\delta_u^*)^2(5s\sigma_g 5s\sigma_u^*)^2 \quad (7)$$

This (orbital) active space resulted in 332 model space CSFs for the $^1\Sigma_g^+$ state (and 1,886,186,600 total CSFs using a aug-cc-pVTZ-DK basis set[57]); 280 model space and 3,192,157,814 total CSFs for the $^5\Sigma_g^+$ state; and 10 model space and 423,682,756 all space CSFs for the $^9\Sigma_g^+$ state. The $4d_z^2$-derived MOs were included with all 3d, 4s, and 4p-derived MOs in the active core and correlated at the GVVPT2 level. For calculations on the $^1\Sigma_g^+$ state involving $5p_z$-dominated MOs, the additional orbitals were added to the σ valence group in MCRM 7. The Mn_2 calculations involved a reference MCRM similar to 7 but with 4s-dominated MOs (instead of the $3d_{z^2}$-derived MOs) placed in the active core together with the 3s- and 3p-dominated MOs.

For the $X^3\Sigma_g^-$ and $1^{11}\Sigma_g^-$ states of Tc_2, the active space included all 4d and 5s-derived MOs grouped as

$$(4d_{xz}\pi_u 4d_{xz}\pi_g^* 4d_{yz}\pi_u 4d_{yz}\pi_g^*)^6(4d_{z^2}\sigma_g 4d_{z^2}\sigma_u^* 4d_{x^2-y^2}\delta_g 4d_{x^2-y^2}\delta_u^* 5s\sigma_g 5s\sigma_u^*)^6(4d_{xy}\delta_g 4d_{xy}\delta_u^*)^2 \quad (8)$$

This partitioning of the model space resulted in 5952 model space and 65,230,481,060 all space CSFs (using aug-cc-pVTZ-DK) for the $X^3\Sigma_g^-$ state, and 2 model space and 975,015,732 total CSFs for the $1^{11}\Sigma_g^-$ state. Although this reference MCRM could be used to construct the Σ_g^+ states of Tc_2, it is obviously more computationally intensive but does not lead to qualitatively (or even semiquantitatively) different PECs. For example, in comparison calculations on the lowest $^1\Sigma_g^+$ state, the single point energy difference from results obtained from using MCRM 7 and 8 was only about 0.006 eV at 2.18 Å (R_e = 2.17 Å for this state). On the other hand, reference MCRM 7 cannot be used to describe the Σ_g^- states of Tc_2. For calculations on the $X^3\Sigma_g^-$ state using $5p_z$-dominated MOs, the additional orbitals were added to the second valence group of MCRM 8.

For all electronic states of Y_2 investigated, the active (orbital) space consisted of 4d (σ and π) and 5s-derived MOs grouped into two orbital subspaces from which three reference MCRMs were constructed as follows.

$$(4d_{xz}\pi_u 4d_{xz}\pi_g^* 4d_{yz}\pi_u 4d_{yz}\pi_g^*)^0(4d_{z^2}\sigma_g 4d_{z^2}\sigma_u^* 5s\sigma_g 5s\sigma_u^*)^6$$
$$(4d_{xz}\pi_u 4d_{xz}\pi_g^* 4d_{yz}\pi_u 4d_{yz}\pi_g^*)^2(4d_{z^2}\sigma_g 4d_{z^2}\sigma_u^* 5s\sigma_g 5s\sigma_u^*)^4$$
$$(4d_{xz}\pi_u 4d_{xz}\pi_g^* 4d_{yz}\pi_u 4d_{yz}\pi_g^*)^4(4d_{z^2}\sigma_g 4d_{z^2}\sigma_u^* 5s\sigma_g 5s\sigma_u^*)^2 \quad (9)$$

This partitioning of the model space gave rise to 172 model space and 1,012,046,286 total (using aug-cc-pVTZ-DK[57]) CSFs used to describe the $1^1\Sigma_g^+$, $2^1\Sigma_g^+$, and $3^1\Sigma_g^+$ states of Y_2. The lowest $^5\Sigma_u^-$ state was described by 58 model space and 1,320,147,234 all space CSFs from these reference MCRMs 9. Preliminary calculations showed that the 4d-derived δ MOs were not important in describing the investigated Y_2 states and were thus excluded from the active space. For calculations on the $1^1\Sigma_g^+$, $2^1\Sigma_g^+$, and $3^1\Sigma_g^+$ states of Y_2 involving $5p_z$-dominated MOs, the orbitals were added to the σ valence group in the reference MCRMs 9.

All calculations (except for Mn_2) were performed in D_{2h} symmetry (with further restriction to $D_{\infty h}$) using an aug-cc-pVTZ-DK basis set, which uses a (25s20p13d3f2g) primitive set contracted to [9s8p6d3f2g] for elements Y to Cd.[57] Mn_2 calculations were performed using atomic natural orbital (ANO) basis sets: ANO-RCC-VTZP,[35] which is a (21s15p10d6f4g) primitive set contracted to [6s5p3d2f1g] and ANO-L VTZP,[58] which has the same size/contraction as the ANO-RCC VTZP basis. Scalar relativistic effects were included through the spin-free exact two-component (sf-X2C) Hamiltonian, with contraction after the picture-change transformation (see section 2.1). Multiconfigurational self-consistent field (MCSCF) calculations were performed using the above referenced MCRMs to account for static electron correlation. At the conclusion of MCSCF calculations, orbitals in invariant groups were rotated into quasi-canonical form. The initial MOs to begin calculations were obtained from approximate natural orbitals of second-order restricted Møller−Plesset perturbation (RMP2) calculations from a closed-shell Hartree−Fock (HF) reference. The dynamic electron correlation energy was obtained through the GVVPT2.

Where reported, the effective bond order (EBO) was determined using the expression

$$\eta = \frac{\sum_i \chi_i {c_i}^2}{\sum_i {c_i}^2} \quad (10)$$

where η is the EBO, χ_i is the EBO for the ith CSF, and c_i^2 is its corresponding weight. The EBO for each important configuration considered was calculated using the well-known formula

$$\chi_i = \frac{1}{2}(n_b - n_{ab}) \quad (11)$$

where n_b denotes the number of bonding and n_{ab} is the number of antibonding electrons.

3. RESULTS AND DISCUSSION

3.1. Y_2: $X^5\Sigma_u^-$, $1^1\Sigma_g^+$, $2^1\Sigma_g^+$, and $3^1\Sigma_g^+$ States. The PECs for the $X^5\Sigma_u^-$ and $1^1\Sigma_g^+$ states of Y_2 are shown in Figure 1 and the data characterizing the curves are shown in Table 1. Similar to the situation in isovalent Sc_2, where two low-lying electronic states ($^5\Sigma_u^-$ and $^3\Sigma_u^-$) are relevant to determination of the ground state, for Y_2 the lowest $^5\Sigma_u^-$ and $^1\Sigma_g^+$ should be

dx.doi.org/10.1021/jp409426n | J. Phys. Chem. A 2014, 118, 1489−1501

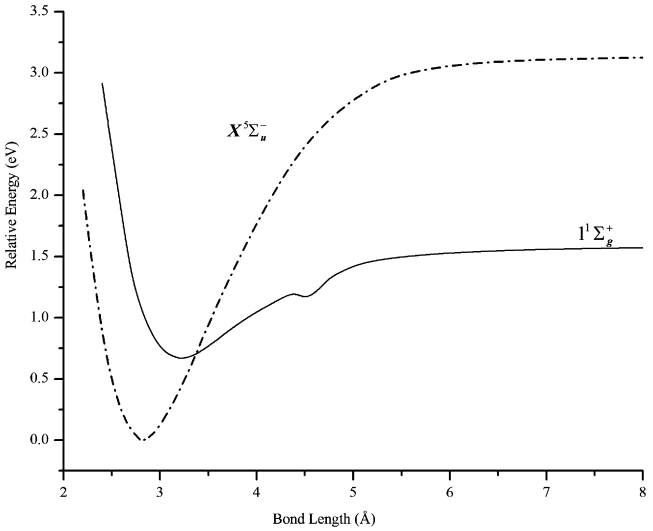

Figure 1. PECs of $X^5\Sigma_u^-$ and $1^1\Sigma_g^+$ states of Y_2 computed at the relativistic GVVPT2 level of theory using the aug-cc-pVTZ-DK basis set. The energies are plotted relative to the lowest energy value of the quintet ground state.

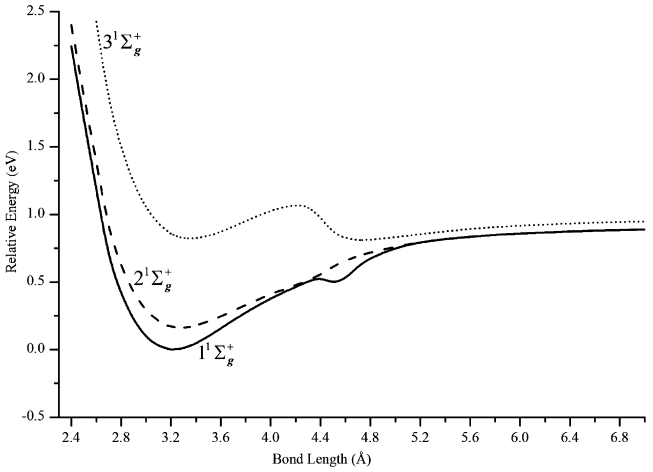

Figure 2. PECs of the $1^1\Sigma_g^+$, $2^1\Sigma_g^+$, and $3^1\Sigma_g^+$ states of Y_2 computed at the relativistic GVVPT2 level of theory using the aug-cc-pVTZ-DK basis set. The energies are plotted relative to the lowest energy of the $1^1\Sigma_g^+$ state.

considered. As mentioned in the Introduction, experimental determination of the symmetry of the Y_2 ground state has not been unambiguous, although a $^5\Sigma_u^-$ ground state seems the more likely. In our study, we found the ground state of the Y_2 molecule to be $^5\Sigma_u^-$, in agreement with most previous theoretical studies (Table 1). In agreement with the Walch and Bauschlicher study,[13] we found the major configuration of the $X^5\Sigma_u^-$ state to be

$$4d_{xz}\pi_u^1 4d_{yz}\pi_u^1 5s\sigma_g^2 4d_{z^2}\sigma_g^1 5s\sigma_u^{*1} \quad (12)$$

For this configuration, we found a weight of 0.800 at 2.80 Å (i.e., at the minimum), which decreased to 0.548 at 4.4 Å. This configuration is quite similar to that often reported for the Sc_2 $X^5\Sigma_u^-$ state. Using formulas 10 and 11 (see above), an EBO of 1.87 was obtained for the ground state of Y_2 at 2.81 Å (using 8 important configurations), which dropped to 1.15 at 4.4 Å. Spectroscopic constants obtained by the GVVPT2 study were in reasonable agreement with the CASSCF/SOCI+Q study[15] and experiment[12] (i.e., R_e = 2.80 Å vs 3.03 vs 2.65; D_e = 3.12 eV vs 2.6 vs 3.5 ± 0.4), although the harmonic frequency was less so (ω_e = 287 cm^{-1} vs 172 vs 184).

We found the $1^1\Sigma_g^+$ state to lie at 0.67 eV above the $X^5\Sigma_u^-$ state around the equilibrium geometry. Walch and Bauschlicher[13] and Dai and Balasubramanian[15] had found the $1^1\Sigma_g^+$ state of Y_2, which had

$$4d_{xz}\pi_u^2 4d_{yz}\pi_u^2 5s\sigma_g^2 \quad (13)$$

as the major configuration, to lie at 0.87 eV above a quintet ground state. They also reported a dissociation asymptote for the singlet state that involved excited Y atoms. In our study, we performed a state averaged calculation on the lowest three $^1\Sigma_g^+$ states of Y_2 with equal weighting and found all three states to correlate with the ground state atoms' dissociation channel. In fact, near degeneracy at certain geometries did not permit even a *qualitatively* correct curve for the $1^1\Sigma_g^+$ state to be computed in a one state calculation. In contrast with the earlier studies, we obtained

$$4d_{xz}\pi_u^2 5s\sigma_g^2 5s\sigma_u^{*2} \quad \text{and} \quad 4d_{yz}\pi_u^2 5s\sigma_g^2 5s\sigma_u^{*2} \quad (14)$$

as the major configurations near the equilibrium bond length. As with the $X^5\Sigma_u^-$ state, spectroscopic constants were in reasonable agreement with the CASSCF/SOCI+Q study[15] (i.e., R_e = 3.21 Å vs 2.76; D_e = 0.91 eV vs 0.37; ω_e = 140 cm^{-1} vs 180; T_e = 0.67 eV vs 0.87); there are not any experiments for this state with which to compare.

The shallow bump around a bond length of 4.6 Å on the $1^1\Sigma_g^+$ PEC shown in Figure 1 is not an artifact but is a consequence of what we suspected to be an avoided crossing. This curve is shown with two other low lying $^1\Sigma_g^+$ states of Y_2 in Figure 2 and the corresponding data describing them are included in Table 1. In particular, our results on the $2^1\Sigma_g^+$ and $3^1\Sigma_g^+$ states of the Y_2 species are the first to be reported, to the best of our knowledge. As can be seen, the PEC for the $3^1\Sigma_g^+$ state has two shallow minima: an inner minimum at R_e = 3.36 Å with D_e = 0.09 eV, ω_e = 118.3 cm^{-1}, and T_e = 0.82 eV (with respect to the $1^1\Sigma_g^+$ state) and an outer very slightly deeper minimum at R_e = 4.72 Å with D_e = 0.10 eV, ω_e = 113.9 cm^{-1}, and T_e = 0.81 eV.

To corroborate the PEC-based hypothesis that the bump in the $1^1\Sigma_g^+$ PEC around 4.6 Å is an avoided crossing, we analyzed the important configurations of the $1^1\Sigma_g^+$ and $2^1\Sigma_g^+$ states just before the bump (at 4.3 Å) and at the bump (4.6 Å). As shown in Table 5, the leading configurations of the $1^1\Sigma_g^+$ state at 4.3 Å (i.e., 1, 4, 7, and 9) become the leading configurations of the $2^1\Sigma_g^+$ state at 4.6 Å (i.e., 1, 2, 3, and 4, respectively), whereas the major configurations of the $2^1\Sigma_g^+$ state at 4.3 Å also become those of the $1^1\Sigma_g^+$ state at 4.6 Å. The configurations shown in Table 5 are represented using step vector notation: the number 0 corresponds to zero orbital occupancy; 1 to single occupancy, spin coupled to increase spin; 2 to single occupancy with a reduction in spin; and 3 to double orbital occupancy. The orbital symmetries (in D_{2h} point group) are {0 0 0 0 1 2 2 3 3 4 5 5 5 5 6 6 7 7 | 2 3 6 7 0 0 5 5} where 0 to 7 denote irreps A_g to B_{3u} with the active core orbitals lexically preceding the valence orbitals. Obtaining the correct initial orbitals for the characterization of these states was difficult. In preliminary state-averaged calculations in which the $5p_z$-derived σ MOs replaced the $4d_{z^2}$-dominated MOs, we found that the $3^1\Sigma_g^+$state correlated with the Y ($4d^25s^1$) + Y ($4d^25s^1$) dissociation asymptote, in violation of the noncrossing rule.

dx.doi.org/10.1021/jp409426n | J. Phys. Chem. A 2014, 118, 1489−1501

Table 5. Important Configurations of the $1^1\Sigma_g^+$ and $2^1\Sigma_g^+$ States of Y_2 Indicative of a Switch in the Two States on Going from 4.3 to 4.6 Å Bond Length[a]

CSF no.	amplitudes	configurations
	$1^1\Sigma_g^+(R = 4.3$ Å)	
1	**0.34157**	**3 0 0 0 3 0 3 0**
2	−0.03741	1 0 0 1 3 2 2 0
3	0.04777	1 0 0 2 3 1 2 0
4	**−0.34157**	**0 3 0 0 3 0 3 0**
5	−0.03741	0 1 1 0 3 2 2 0
6	0.04777	0 1 2 0 3 1 2 0
7	**0.54083**	**0 0 3 0 3 0 3 0**
8	−0.05873	0 0 3 0 0 3 3 0
9	**−0.54083**	**0 0 0 3 3 0 3 0**
10	0.05873	0 0 0 3 0 3 3 0
	$2^1\Sigma_g^+(R = 4.3$ Å)	
1	**−0.28202**	**0 0 0 0 3 3 3 0**
2	**0.07568**	**0 0 0 0 3 0 3 3**
3	**−0.33449**	**3 0 0 0 3 0 3 0**
4	**−0.33449**	**0 3 0 0 3 0 3 0**
5	**0.50751**	**0 0 3 0 3 0 3 0**
6	**0.50751**	**0 0 0 3 3 0 3 0**
7	−0.06378	0 0 3 3 0 0 3 0
	$1^1\Sigma_g^+(R = 4.6$ Å)	
1	**0.65995**	**0 0 0 0 3 3 3 0**
2	−0.05299	0 0 0 0 3 3 1 2
3	**−0.39146**	**0 0 0 0 3 0 3 3**
4	0.06181	0 0 0 0 1 2 3 3
5	**0.22319**	**3 0 0 0 3 0 3 0**
6	**0.22319**	**0 3 0 0 3 0 3 0**
7	**−0.27683**	**0 0 3 0 3 0 3 0**
8	**−0.27683**	**0 0 0 3 3 0 3 0**
	$2^1\Sigma_g^+(R = 4.3$ Å)	
1	**0.39767**	**3 0 0 0 3 0 3 0**
2	**-0.39767**	**0 3 0 0 3 0 3 0**
3	**0.51141**	**0 0 3 0 3 0 3 0**
4	**-0.51141**	**0 0 0 3 3 0 3 0**

[a]Active core orbitals are fully occupied in all listed configurations. Configurations of the states that get exchanged are shown in bold (e.g., configurations 1, 4, 7, and 9 of state $1^1\Sigma_g^+$ at 4.3 Å become configurations 1, 2, 3, and 4, respectively of state $2^1\Sigma_g^+$ at 4.6 Å).

With the use of formulas 10 and 11, the EBO for the $1^1\Sigma_g^+$ state was 0.90 (using 10 important configurations), for $2^1\Sigma_g^+$ 0.94 (using 12 important configurations), and for $3^1\Sigma_g^+$ 0.94 (using 10 important configurations) at 3.24 Å. At this geometry, two leading configurations for the $1^1\Sigma_g^+$ state, each contributing 0.381 by weight to the wave function, were $4d_{xz}\pi_u^2 5s\sigma_g^2 5s\sigma_u^{*2}$ and $4d_{yz}\pi_u^2 5s\sigma_g^2 5s\sigma_u^{*2}$. The same configurations were also major in the $2^1\Sigma_g^+$ state, contributing 0.353 by weight each to the overall wave function. The leading configuration for the $3^1\Sigma_g^+$ state was $5s\sigma_g^2 4d_{z^2}\sigma_g^2 5s\sigma_u^{*2}$, contributing 0.756 by weight to the wave function at 3.24 Å. It is important to note that all these configurations suggest the coupling of two ground Y atoms (Y: $4d^1 5s^2$).

When the $5p_z$-dominated MOs in the state-averaged calculations were included on the $1^1\Sigma_g^+$, $2^1\Sigma_g^+$, and $3^1\Sigma_g^+$ states of Y_2, the bump in the $1^1\Sigma_g^+$ curve was seen to be shifted inward to around 3.0 Å bond length whereas the inner minimum in the $3^1\Sigma_g^+$ curve now lay around 2.9 Å (Figure 3). A few calculations were performed involving four $^1\Sigma_g^+$ states of Y_2 around the bump in the $3^1\Sigma_g^+$ curve and the latter curve was found to be

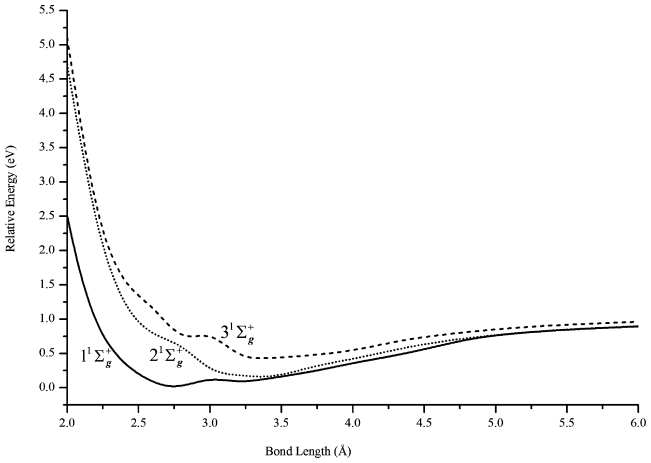

Figure 3. PECs of the $1^1\Sigma_g^+$, $2^1\Sigma_g^+$, and $3^1\Sigma_g^+$ states of Y_2 computed at the relativistic GVVPT2 level of theory using the aug-cc-pVTZ-DK basis set and an active space that included $5p_z$-derived MOs. The energies are plotted relative to the lowest energy of the $1^1\Sigma_g^+$ state.

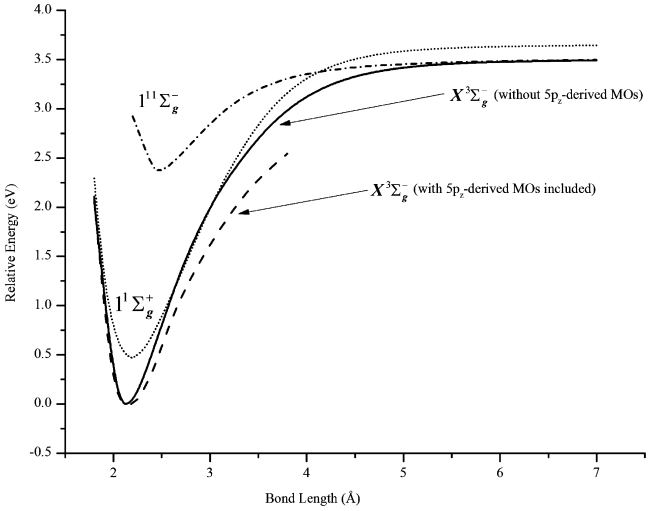

Figure 4. PECs of the $X^3\Sigma_g^-$, $1^1\Sigma_g^+$, and $1^{11}\Sigma_g^-$ states of Tc_2 computed at the relativistic GVVPT2 level of theory using the aug-cc-pVTZ-DK basis set. The energies are plotted relative to the lowest energy value of the $X^3\Sigma_g^-$ state. A partial curve for the ground state computed with $5p_z$-derived MOs included in the active space is also shown.

energetically quite close to the $4^1\Sigma_g^+$ curve, indicating a likely avoided crossing that might explain the double minimum in the $3^1\Sigma_g^+$ curve.

3.2. Electronic States of Tc_2 and Mn_2. The PECs obtained for the $X^3\Sigma_g^-$, $1^{11}\Sigma_g^-$, $1^1\Sigma_g^+$, $1^5\Sigma_g^+$, and $1^9\Sigma_g^+$ states of Tc_2 are shown in Figures 4–6, with additional data describing the curves featured in Table 2 in which spin-free relativistic GVVPT2 results are compared with results from other methods. Unlike Mn_2 (Figure 7 and Table 6, which also contains some experimental results[59–61]) with a $X^1\Sigma_g^+$ ground state, the ground state of Tc_2 was found to be $^3\Sigma_g^-$ as was observed also by, e.g., Yanagisawa et al.[16] and Borin et al.[24] This state was found to be strongly bound, with a binding energy (D_e = 3.50 eV) comparable to experimental results (i.e., 2.93–3.49 eV). At the equilibrium geometry (2.13 Å), the leading configuration for the $X^3\Sigma_g^-$ term was found to be

dx.doi.org/10.1021/jp409426n | J. Phys. Chem. A 2014, 118, 1489–1501

$$4d_{xz}\pi_u^2 4d_{xz}\pi_g^{*1} 4d_{yz}\pi_u^2 4d_{yz}\pi_g^{*1} 4d_{z^2}\sigma_g^2 5s\sigma_g^2 4d_{x^2-y^2}\delta_g^2 4d_{xy}\delta_g^2 \quad (15)$$

which is similar to that obtained by Klyagina et al.,[28,29]

$$5s\sigma_g^2 4d_{z^2}\sigma_g^2 4d_{xz}\pi_u^2 4d_{x^2-y^2}\delta_g^2 4d_{xy}\delta_g^2 4d_{x^2-y^2}\delta_u^{*1} 4d_{xy}\delta_u^{*1} \quad (16)$$

and the average orbital occupations by Borin et al.,[24]

$$8\sigma_g(d\sigma)^{1.89} 2\delta_g(d\delta)^{3.79} 9\sigma_g(5s)^{1.91} 5\pi_u(d\pi)^{3.78} 8\sigma_u^*(d\sigma)^{0.12} 2\delta_u^*(d\delta)^{2.19} 9\sigma_u^*(5s)^{0.09} 5\pi_g^*(d\pi)^{0.23} \quad (17)$$

all suggesting a quintuple bond. At R_e = 2.13 Å, we used 61 CSFs with weights in the range [0.001, 0.306] to compute an EBO of 3.65 for the $X^3\Sigma_g^-$ state of Tc_2. Relativistic effects, which are expected to slightly contract the s and p while expanding the d and f atomic orbitals, imply that the 4d and 5s orbitals of Tc could have about the same spatial extent and could both be involved in bonding (N.B. the 5s → 5d excitation energy is only 0.41 eV[23]). At the (scalar relativistic) CASSCF/CASPT2 level,[24] the $X^3\Sigma_g^-$ state had R_e = 1.94 Å, ω_e = 492.0 cm^{-1}. At the GVVPT2 level, we obtained R_e = 2.13 Å and ω_e = 336.6 cm^{-1}. Consideration of a larger active space including $5p_z$-derived MOs did not appear to change the PEC of the $X^3\Sigma_g^-$ state qualitatively in the chemically important region of the curve (Figure 4). Such expensive calculations involved a total space dimension of as large as 232,091,673,238 CSFs.

The $1^1\Sigma_g^+$ state of Tc_2 was found to be 0.47 eV less stable than the $X^3\Sigma_g^-$ state around the equilibrium geometry and had R_e = 2.19 Å, ω_e = 253.9 cm^{-1}, and D_e = 3.18 eV with the aug-cc-pVTZ-DK basis. The configurational structure of the $1^1\Sigma_g^+$ state was found to be extremely mixed to the extent that the leading configuration (at 2.18 Å),

$$4d_{xz}\pi_u^2 4d_{yz}\pi_u^2 4d_{z^2}\sigma_g^2 4d_{z^2}\delta_u^{*2} 5s\sigma_g^2 4d_{x^2-y^2}\delta_g^2 4d_{xy}\delta_g^2 \quad (18)$$

contributed only 0.209 by weight to the overall wave function. The weight of this configuration decreased to 0.009 at 4.1 Å, where the leading configuration became

$$4d_{xz}\pi_u^1 4d_{xz}\pi_g^{*1} 4d_{yz}\pi_u^1 4d_{yz}\pi_g^{*1} 4d_{z^2}\sigma_g^2 4d_{z^2}\sigma_u^{*2} 5s\sigma_g^2 4d_{x^2-y^2}\delta_g^1 4d_{x^2-y^2}\delta_u^{*1} 4d_{xy}\delta_g^1 4d_{xy}\delta_u^{*1} \quad (19)$$

with a weight of only 0.014. At 2.18 Å, we used 67 important CSFs to compute the EBO of the $1^1\Sigma_g^+$ state of Tc_2 and obtained 3.17. The $1^1\Sigma_g^+$ state of Tc_2 was also computed using a larger active space that included $5p_z$-dominated MOs. As can be seen in Figure 5, the two PECs with and without $5p_z$-derived MOs are quite similar whereas the larger active space increased the total space dimension from 881,588,512 to 3,704,894,420 CSFs (using cc-pVTZ-DK).

Relativistic effects can be seen when not just the binding strengths of Mn_2 and Tc_2 but also their bond lengths are compared. Taking into account that the atomic radii of Mn and Tc are close (i.e., 1.40 and 1.35 Å, respectively), it is remarkable that the bond length of the $1^1\Sigma_g^+$ state of Tc_2 is dramatically different (i.e., at least 1.0 Å less) than that of the $X^1\Sigma_g^+$ state of Mn_2 (Tables 2 and 6). Figure 8 contains PECs for the $X^1\Sigma_g^+$ state of Mn_2 computed with ANO-type basis sets and a Dunning type cc-pVQZ basis. The ANO-type basis sets prove to be better at predicting the bond length and binding energy of the Mn_2 ground state compared with the Dunning type basis. After relativistic effects were included, a slight elongation was observed in the Mn_2 bond length (by 0.02 Å) when the ANO-RCC VTZP basis set is used.

One DFT study[31] found the spin polarized $1^{11}\Sigma_g^-$ state to be the ground state of Tc_2 with R_e = 2.84 Å, ω_e = 178.5 cm^{-1}, and D_e = 2.27 eV. In our calculations, this state was found to lie as far as 2.38 eV above the ground state (at the equilibrium geometry) and had R_e = 2.47 Å, ω_e = 225.1 cm^{-1}, and D_e = 1.13 eV. At a bond length of 2.48 Å, this state was described by two leading configurations:

$$4d_{xz}\pi_u^2 4d_{xz}\pi_g^{*1} 4d_{yz}\pi_u^2 4d_{yz}\pi_g^{*1} 4d_{z^2}\sigma_g^1 4d_{z^2}\sigma_u^{*1} 5s\sigma_g^1 5s\sigma_u^{*1} 4d_{x^2-y^2}\delta_g^1 4d_{x^2-y^2}\delta_u^{*1} 4d_{xy}\delta_g^1 4d_{xy}\delta_u^{*1}$$

$$4d_{xz}\pi_u^1 4d_{xz}\pi_g^{*2} 4d_{yz}\pi_u^1 4d_{yz}\pi_g^{*2} 4d_{z^2}\sigma_g^1 4d_{z^2}\sigma_u^{*1} 5s\sigma_g^1 5s\sigma_u^{*1} 4d_{x^2-y^2}\delta_g^1 4d_{x^2-y^2}\pi_u^{*1} 4d_{xy}\delta_g^1 4d_{xy}\delta_u^{*1}$$

with weights of 0.669 and 0.121, respectively. At this geometry, the EBO was 0.694. These configurations continued to be the leading ones with their weights becoming equal at elongated bond lengths.

Figure 6 contains the PECs of the $1^1\Sigma_g^+$, $1^5\Sigma_g^+$, and $1^9\Sigma_g^+$ states of Tc_2 obtained at the GVVPT2 level, whereas Figure 7 contains the PECs of the same states for the isovalent Mn_2 species. Though these states are virtually degenerate in the case of Mn_2, a relativistic treatment of Tc_2 shows them to be significantly nondegenerate, the $1^5\Sigma_g^+$ and $1^9\Sigma_g^+$ states being found to be 0.70 and 1.84 eV less stable than the $1^1\Sigma_g^+$ state, respectively.

The calculations performed on the $1^5\Sigma_g^+$ and $1^9\Sigma_g^+$ states of Tc_2 seem to be the first reported. The leading configuration of the $1^5\Sigma_g^+$ state is

$$4d_{xz}\pi_u^2 4d_{yz}\pi_u^2 4d_{z^2}\sigma_g^2 4d_{z^2}\sigma_u^{*2} 5s\sigma_g^2 4d_{x^2-y^2}\delta_g^1 4d_{x^2-y^2}\delta_u^{*1} 4d_{xy}\delta_g^1 4d_{xy}\delta_u^{*1}$$

dx.doi.org/10.1021/jp409426n | J. Phys. Chem. A 2014, 118, 1489−1501

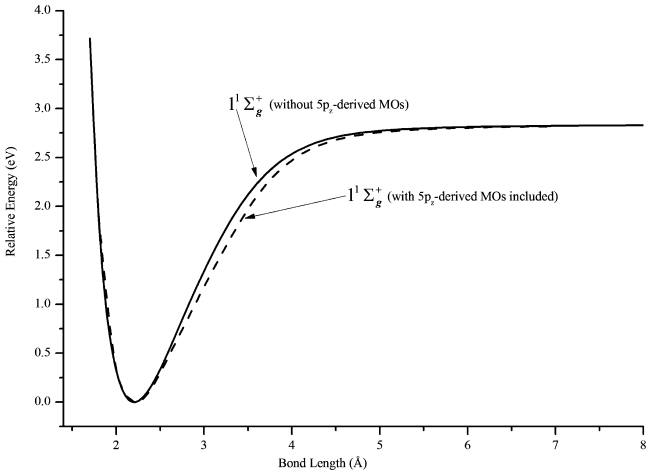

Figure 5. PECs of the $1^1\Sigma_g^+$ state of Tc_2 computed at the relativistic GVVPT2 level of theory using the cc-pVTZ-DK basis set with and without inclusion of the $5p_z$-derived MOs.

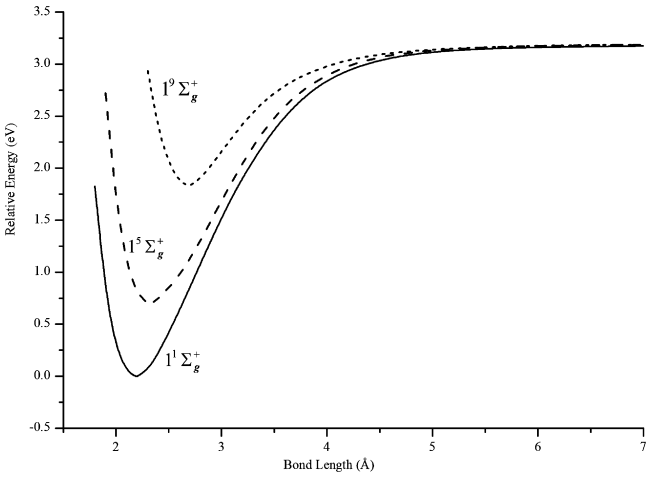

Figure 6. PECs of the $1^1\Sigma_g^+$, $1^5\Sigma_g^+$, and $1^9\Sigma_g^+$ states of Tc_2 computed at the relativistic GVVPT2 level of theory using the aug-cc-pVTZ-DK basis set. The energies are plotted relative to the lowest energy value of the $1^1\Sigma_g^+$ state.

Table 6. Equilibrium Distances (R_e), Binding Energies (D_e), and Harmonic Frequencies (ω_e) of the $X^1\Sigma_g^+$ Electronic State of Mn_2 Calculated Using Nonrelativistic and Spin-Free X2C Relativistic GVVPT2 Compared with Experiment

method	basis set	R_e (Å)	D_e (eV)	ω_e (cm^{-1})
GVVPT2[a]	cc-pVQZ	3.83	0.05	30.7
GVVPT2	ANO-L-VTZP	3.45	0.21	31.4
GVVPT2[b]	ANO-RCC-VTZP	3.57	0.15	27.2
GVVPT2[c]	ANO-RCC-VTZP	3.59	0.13	25.7
experiment		3.40[d]	0.02−0.15[e]	68.1[f]

[a]Previous nonrelativistic calculations (ref 38). [b]Nonrelativistic. [c]Relativistic. [d]Reference 59. [e]Reference 60. [f]Reference 61.

with a weight of 0.257 at 2.31 Å. This weight decreased to 0.009 at 5.0 Å where the leading configuration was the same as that reported above at 4.10 Å for the $1^1\Sigma_g^+$ state (i.e., (19)) and had a weight of only 0.012. Using 99 CSFs with amplitudes in the range [0.100, 0.507], we computed an EBO of 0.87 at 2.68 Å

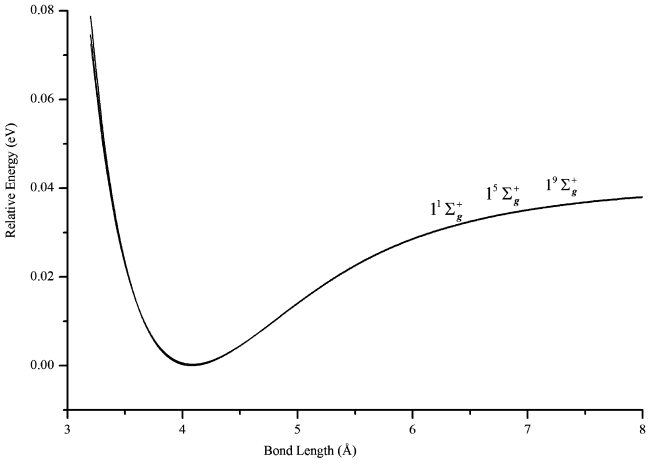

Figure 7. PECs of the $1^1\Sigma_g^+$, $1^5\Sigma_g^+$, and $1^9\Sigma_g^+$ states of Mn_2 computed at the GVVPT2 level of theory using the cc-pVTZ basis set. All three states are virtually degenerate at all geometries.

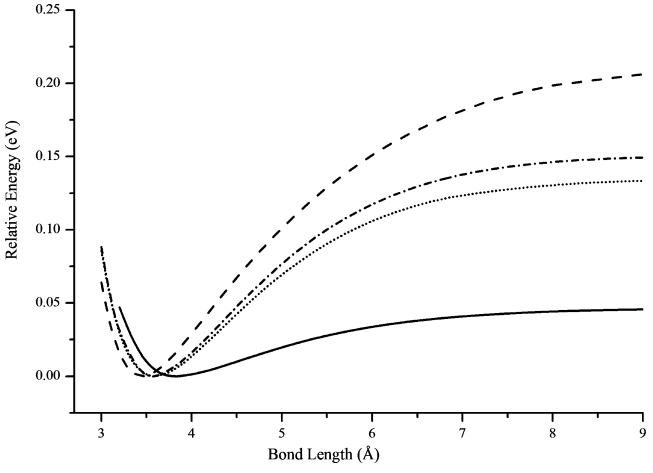

Figure 8. PECs of the $X^1\Sigma_g^+$ state of Mn_2 computed at the GVVPT2 level of theory using cc-pVQZ (solid line), ANO-RCC VTZP with sf-X2C (dotted), ANO-RCC VTZP (dash-dot) and ANO-L VTZP (dashed).

for the $1^5\Sigma_g^+$ state of Tc_2. The leading configuration for the $1^9\Sigma_g^+$ state of Tc_2 at 2.68 Å was again 19 with a weight of 0.694. This weight decreased to only 0.114 at 4.7 Å where 10 important configurations were found to have nearly equal weights. At 2.68 Å and using 10 CSFs with amplitudes in the range [0.081, 0.833], the EBO was computed to be 0.87 for the $1^9\Sigma_g^+$ state of Tc_2.

4. CONCLUSIONS

This paper describes the full PECs of the ground electronic states of Y_2 and Tc_2 and some of their low lying excited states as were obtained at the GVVPT2 level of theory with relativistic effects included via the spin-free exact two-component (sf-X2C) Hamiltonian. In particular, the simple model spaces motivated by valence bond-type active spaces, which we found to nicely describe first-row TM dimers,[38] have also proven to work well for second-row TM dimers. Our results on the Y_2 states are quite revealing of how complicated this seemingly simple species with only 6 active electrons are. Whereas previous theoretical studies considered the $1^1\Sigma_g^+$ state of Y_2, only Dai and Balasubramanian[15] reported a dissociation

asymptote involving two ground Y atoms for this state (in addition to a dissociation channel involving excited state atoms) but did not provide a full PEC. Our study is the first to find that the lowest three $^1\Sigma_g^+$ states of Y_2 correlate with the ground state atoms' dissociation limit, as expected theoretically. Although the lowest two $^1\Sigma_g^+$ states were described reasonably well with an active (orbital) space of 4d (σ and π) and 5s-derived MOs, inclusion of $5p_z$-derived orbitals provides better curves. In contrast, computational artifacts remain for $3^1\Sigma_g^+$, which suggests that the states originating from the first excited dissociation limit should be included for quantitative studies of that state. Overall, even though the ground term for the Y_2 molecule has not been experimentally determined unambiguously, many theoretical studies have tended to favor a $^5\Sigma_u^-$ ground state and our present work lends further support in this regard. Comparison of GVVPT2 results with those from CASSCF/SOCI+Q and experiment, where available, corroborate the general correctness of our results, but also suggest that more accurate calculations are needed especially for spectroscopic studies.

A comparison between the Mn_2 and Tc_2 electronic states illustrated the importance of relativistic effects. As was shown, these effects are weak in the case of Mn but strong in Tc, resulting in different bonding situations, different ground terms for Mn_2 and Tc_2, and generally shorter bond lengths in the states of Tc_2 compared with those of Mn_2. For example, the bond length of the $1^1\Sigma_g^+$ state of Tc_2 is dramatically different (i.e., at least 1.0 Å less) from that of the $X^1\Sigma_g^+$ state of Mn_2, despite the closeness of the atomic radii (i.e., 1.40 and 1.35 Å).

In contrast to a 2001 MP2 study[16] that predicted the ground state of Tc_2 to be $^7\Pi_u$, a 2004 DFT study[31] that predicted $^{11}\Sigma_g^-$, and in corroboration of a 2009 CASPT2 study[24] that predicted a $^3\Sigma_g^-$ ground state, our spin-free X2C GVVPT2 calculations predict a $^3\Sigma_g^-$ ground state (R_e = 2.13 Å, ω_e = 336.6 cm^{-1}, and D_e = 3.50 eV) with a low-lying (0.47 eV) $^1\Sigma_g^+$ state (R_e = 2.19 Å, ω_e = 253.9 cm^{-1}, and D_e = 3.18 eV). Although the 2009 CASPT2 study showed strong spin−orbit induced mixing between the $^3\Sigma_g^-$ and $^1\Sigma_g^+$ states, the spectroscopic constants they obtained from the spin-free PECs did not change much with inclusion of spin−orbit coupling. On comparison of spin-free PECs, our calculations suggest a somewhat longer (ca. 0.15 Å) and broader (ca. 100 cm^{-1}) minimum. Whether this is due to treatment of correlation (including choice of H_0) or some other effect remains to be determined. In addition to calculations on the lowest $^3\Sigma_g^-$, $1^1\Sigma_g^+$, and $1^{11}\Sigma_g^-$ curves, we reported herein the apparently first studies of the relatively low-lying $1^5\Sigma_g^+$ and $1^9\Sigma_g^+$ states (i.e., 0.70 and 1.84 eV above $1^1\Sigma_g^+$, respectively). These states were found to be bound (2.49 and 1.35 eV, respectively; effective bond orders ca. 0.9) with slightly elongated bond lengths relative to $^3\Sigma_g^-$ and $^1\Sigma_g^+$. It is expected that the GVVPT2 characterization of the low-lying electronic states of Tc_2 will facilitate the up-to-now unknown experimental results and assist with identifying potentially interesting targets for more computationally intensive methods (e.g., MRCISD, CCSD(T)).

This study represents the first use of GVVPT2 on second-row transition metals in conjunction with the spin-free X2C Hamiltonian. Having observed general agreement with other established approaches where data were available, it was shown that questions concerning potential energy surfaces that were simply not available beforehand can now be addressed. For example, this was the first study to obtain the $2^1\Sigma_g^+$and $3^1\Sigma_g^+$ curves of Y_2, which prove to be critical in understanding the dissociation channels. We anticipate that more such results will be forthcoming.

■ ASSOCIATED CONTENT

Supporting Information

Five tables are available that provide exact abscissa and ordinates used in constructing PECs in Figures 1−4 and 6 and 7. This material is available free of charge via the Internet at http://pubs.acs.org.

■ AUTHOR INFORMATION

Corresponding Authors

*M. R. Hoffmann: e-mail, mhoffmann@chem.und.edu.
*W. Liu: e-mail, liuwjbdf@gmail.com.

Notes

The authors declare no competing financial interest.

■ ACKNOWLEDGMENTS

P.K.T. and M.R.H. are grateful to the (US) NSF (Grant No. EPS-0814442) and Z.L. and W.L. to the National Natural Science Foundation of China (Project No. 21033001, 21273011, and 21290192) for financial support.

■ REFERENCES

(1) Klyagina, A. P.; Fursova, V. D.; Levin, A. A.; Gutsev, G. L. Electronic Structure and Chemical Bond in the Technetium Dimer. *Dokl. Akad. Nauk. SSSR* **1987**, *292*, 122−125.

(2) Alberto, R. New Organometallic Technetium Complexes for Radiopharmaceutical Imaging. *Top Curr. Chem.* **2005**, *252*, 1−44.

(3) Morschhauser, F.; Radford, J.; Hoof, A. V.; Vitolo, U.; Soubeyran, P.; Tilly, H.; Huijgens, P. C.; Kolstad, A.; d'Amore, F.; Diaz, M. G.; et al. Phase III Trial of Consolidation Therapy with Yttrium-90−Ibritumomab Tiuxetan Compared with No Additional Therapy After First Remission in Advanced Follicular Lymphoma. *J. Clin. Oncol.* **2008**, *26*, 5156−5164.

(4) http://chemistry.about.com/od/elementfacts/a/yttrium.htm. Yttrium Facts. (accessed: 12/02/2012).

(5) Noddack, W.; Tacke, I.; Berg, O. Die Ekamangane. *Naturwis.* **1925**, *13*, 567−574.

(6) de Jonge, F. A. A.; Pauwels, E. K. J. Technetium, the Missing Element. *Eur. J. Nucl. Med.* **1996**, *23*, 336−344.

(7) Armstrong, J. T. Technetium. *Chem. Eng. News* **2003**, *81*, 110.

(8) Poineau, F.; Sattelberger, A. P.; Czerwinski, K. R. XAFS Spectroscopic Study of $Tc_2(O_2CCH_3)_4X_2$ (X = Cl, Br). *J. Coord. Chem.* **2008**, *61*, 2356−2370.

(9) Verhaegen, G.; Smoes, S.; Drowart, J. Mass-Spectrometric Determination of the Dissociation Energy of the Molecules Sc_2, Y_2, La_2, and YLa. *J. Chem. Phys.* **1964**, *40*, 239−241.

(10) Knight, L. B.; Woodward, R. W.; Van Zee, R. J.; Weltner, W. Properties of Sc_3, Y_3, and Sc_{13} Molecules at Low Temperatures, as Determined by ESR. *J. Chem. Phys.* **1983**, *79*, 5820−5827.

(11) Yang, D. S.; Simard, B.; Hackett, P. A.; Bréces, A.; Zgierski, M. Z. Diyttrium: Evidence for a $^5\Sigma_u^-$ Ground State from Pulsed-Field Ionization Zero Electron Kinetic Energy Photoelectron Spectroscopy and Density Functional Calculations. *Int. J. Mass Spectrom. Ion Processes* **1996**, *159*, 65−74.

(12) Fang, L.; Shen, C.; Liu, Y.; Lindsay, D. M.; Lombardi, J. R. Spectroscopy of Yttrium Dimers in Argon Matrices. *Low Temp. Phys.* **2000**, *26*, 752−755.

(13) Walch, S. P.; Bauschlicher, C. W., Jr. Theoretical Studies of Transition Metal Dimers. In *Comparison of ab initio Quantum Chemistry with Experiment for Small Molecules*; Barlett, R. J., Ed.; Reidel: Amsterdam, Holland, 1985; pp 17−51.

(14) Kalemos, A.; Kaplan, I. G.; Mavridis, A. The Sc_2 Dimer Revisited. *J. Chem. Phys.* **2010**, *132*, 024309/1−7.

(15) Dai, D.; Balasubramanian, K. Electronic States of Y_n (n = 2−4). *J. Chem. Phys.* **1993**, *98*, 7098−7106.
(16) Yanagisawa, S.; Tsuneda, T.; Hirao, K. Investigation of the Use of Density Functionals in Second- and Third-Row Transition Metal Dimer Calculations. *J. Comput. Chem.* **2001**, *22*, 1995−2009.
(17) Wu, Z. J. Density Functional Study of the Second Row Transition Metal Dimers. *Chem. Phys. Lett.* **2004**, *383*, 251−255.
(18) Cotton, F. A.; Fanwick, P. E.; Gage, L. D. Tetra (2-Oxopyridinato) Chloroditechnitium. A New Compound with a Technetium-Technetium Bond of Order 3.5 and a Remarkable Vibronic Absorption Spectrum. *J. Am. Chem. Soc.* **1980**, *102*, 1570−1577.
(19) Cotton, F. A.; Shive, L. W. Structure of Tripotassium Octachloroditechnetate Hydrate. *Inorg. Chem.* **1975**, *14*, 2032−2035.
(20) Poineau, F.; Johnstone, E. V.; Weck, P. F.; Forster, P. M.; Kim, E.; Czerwinski, K. R.; Sattelberger, A. P. β-Technetium Trichloride: Formation, Structure, and First-Principles Calculations. *Inorg. Chem.* **2012**, *51*, 4915−4917.
(21) Poineau, F.; Mausolf, E.; Jarvinen, G. D.; Sattelberger, A. P.; Czerwinski, K. R. Technetium Chemistry in the Fuel Cycle: Combining Basic and Applied Studies. *Inorg. Chem.* **2013**, *52*, 3573−3578.
(22) Cotton, F. A.; Walton, R. A. *Multiple Bonds Between Metal Atoms*; Wiley: New York, 1982.
(23) Morse, M. D. Clusters of Transition-Metal Atoms. *Chem. Rev.* **1986**, *86*, 1049−1109.
(24) Borin, A. C.; Gobbo, J. P.; Roos, B. O. Electronic Structure and Chemical Bonding in the Ground States of Tc_2 and Re_2. *Mol. Phys.* **2009**, *107*, 1035−1040.
(25) Palmeri, P.; Wyart, J. Interpretation of Energy Levels and Predicted Transition Probabilities in Neutral Technetium (TcI). *J. Quant. Spectrosc. Radiat. Transfer* **1999**, *61*, 603−616.
(26) Miedema, A. R.; Gingerich, K. A. On the Formation Enthalpy of Metallic Dimers. *J. Phys. B* **1979**, *12*, 2081−2095.
(27) Brewer, L.; Winn, J. S. Models for Calculation of Dissociation Energies of Homonuclear Diatomic Molecules. *Faraday Symp. Chem. Soc.* **1980**, *14*, 126−135.
(28) Klyagina, A. P.; Fursova, V. D.; Levin, A. A.; Gutsev, G. L. The Chemical Bond in Dimers of Group V and Group VII Transition Metals. *Zh. Strukt. Khim.* **1985**, *28*, 39−45.
(29) Klyagina, A. P.; Fursova, V. D.; Levin, A. A.; Gutsev, G. L. The Chemical Bond in Dimers of Group V and Group VII Transition Metals. *J. Struct. Chem.* **1987**, *28*, 31−37.
(30) Sekine, R.; Kondo, R.; Yamamoto, T.; Onoe, J. Geometric and Electronic Structures of Tc and Mn Clusters by Density Functional Calculations. *Radiochem.* **2003**, *45*, 233−236.
(31) Yan, S.-Y.; Zhu, Z.-H. Spin Polarization Effect for Tc_2 Molecule. *Chin. Phys. B* **2004**, *13*, 2053−2057.
(32) Douglas, M.; Kroll, N. M. Quantum Electrodynamical Corrections to the Fine Structure of Helium. *Ann. Phys.* **1974**, *82*, 89−155.
(33) Hess, B. A. Relativistic Electronic-structure Calculations Employing a 2-Component No-Pair Formalism with External-Field Projection Operators. *Phys. Rev. A* **1986**, *33*, 3742−3748.
(34) Jansen, G.; Hess, B. A. Revision of the Douglas-Kroll Transformation. *Phys. Rev. A* **1989**, *39*, 6016−6017.
(35) Roos, B. O.; Lindh, R.; Malmqvist, P. A.; Veryazov, V.; Widmark, P. O. New Relativistic ANO Basis Sets for Transition Metal Atoms. *J. Phys. Chem. A* **2005**, *109*, 6575−6579.
(36) Khait, Y. G.; Song, J.; Hoffmann, M. R. Explication and Revision of Generalized Van Vleck Perturbation Theory for Molecular Electronic Structure. *J. Chem. Phys.* **2002**, *117*, 4133−4145.
(37) Jiang, W.; Khait, Y. G.; Hoffmann, M. R. Configuration-Driven Unitary Group Approach for Generalized Van Vleck Variant Multireference Perturbation Theory. *J. Phys. Chem. A* **2009**, *113*, 4374−4380.
(38) Tamukong, P. K.; Theis, D.; Khait, Y. G.; Hoffmann, M. R. GVVPT2 Multireference Perturbation Theory Description of Diatomic Scandium, Chromium, and Manganese. *J. Phys. Chem. A* **2012**, *116*, 4590−4601.
(39) Liu, W. Ideas of Relativistic Quantum Chemistry. *Mol. Phys.* **2010**, *108*, 1679−1706.
(40) Cheng, L.; Gauss, J. Analytic Energy Gradients for the Spin-Free Exact Two-Component Theory Using an Exact Block Diagonalization for the One-Electron Dirac Hamiltonian. *J. Chem. Phys.* **2011**, *135*, 084114/1−7.
(41) Li, Z.; Suo, B.; Zhang, Y.; Xiao, Y.; Liu, W. Combining Spin-Adapted Open-Shell TD-DFT with Spin−Orbit Coupling. *Mol. Phys.* **2013**, *111*, 3741−3755.
(42) Li, Z.; Xiao, Y.; Liu, W. On the Spin Separation of Algebraic Two-Component Relativistic Hamiltonians. *J. Chem. Phys.* **2012**, *137*, 154114/1−18.
(43) Dyall, K. G. Interfacing Relativistic and Nonrelativistic methods. I. Normalized Elimination of the Small Component in the Modified Dirac Equation. *J. Chem. Phys.* **1997**, *106*, 9618−9626.
(44) Liu, W.; Peng, D. Exact Two-Component Hamiltonians Revisited. *J. Chem. Phys.* **2009**, *131*, 031104/1−4.
(45) Liu, W.; Peng, D. Infinite-Order Quasirelativistic Density Functional Method Based on the Exact Matrix Quasirelativistic Theory. *J. Chem. Phys.* **2006**, *125*, 044102/1−10; *125*, 149901(E).
(46) Peng, D.; Liu, W.; Xiao, Y.; Cheng, L. Making Four- and Two-Component Relativistic Density Functional Methods Fully Equivalent Based on the Idea of "From Atoms to Molecule. *J. Chem. Phys.* **2007**, *127*, 104106/1−15.
(47) Peng, D.; Reiher, M. Local Relativistic Exact Decoupling. *J. Chem. Phys.* **2012**, *136*, 244108/1−11.
(48) Roos, B. O.; Lindh, R.; Malmqvist, P.-Å.; Veryazov, V.; Widmark, P.-O. Main Group Atoms and Dimers Studied with a New Relativistic ANO Basis Set. *J. Phys. Chem. A* **2005**, *108*, 2851−2858.
(49) Sun, Q.; Xiao, Y.; Liu, W. Exact Two-Component Relativistic Theory for NMR Parameters: General Formulation and Pilot Application. *J. Chem. Phys.* **2012**, *137*, 174105/1−20.
(50) Hoffmann, M. R.; Datta, D.; Das, S.; Mukherjee, D.; Szabados, A.; Rolik, Z.; Surján, P. R. Comparative Study of Multireference Perturbative Theories for Ground and Excited States. *J. Chem. Phys.* **2009**, *131*, 204104/1−11.
(51) Mbote, Y. E. B.; Khait, Y. G.; Hardel, C.; Hoffmann, M. R. Multireference Generalized Van Vleck Perturbation Theory (GVVPT2) Study of the NCO + HCNO Reaction: Insight into Intermediates. *J. Phys. Chem. A* **2010**, *114*, 8831−8836.
(52) Mokambe, R. M.; Khait, Y. G.; Hoffmann, M. R. Ground and Low-Lying Excited Electronic States of [3,3′] Bidiazirinylidene (C_2N_4). *J. Phys. Chem. A* **2010**, *114*, 8119−8125.
(53) Mokambe, R. M.; Hicks, J. M.; Kerker, D.; Jiang, W.; Theis, D.; Chen, Z.; Khait, Y. G.; Hoffmann, M. R. GVVPT2Multireference Perturbation Theory Study of Selenium Oxides. *Mol. Phys.* **2013**, *111*, 1078−1091.
(54) Camacho, C.; Witek, H. A.; Yamamoto, S. Intruder States in Multireference Perturbation Theory: The Ground State of Manganese Dimer. *J. Comput. Chem.* **2009**, *30*, 468−478.
(55) Khait, Y. G.; Song, J.; Hoffmann, M. R. Macroconfigurations in Molecular Electronic Structure Theory. *Int. J. Quantum Chem.* **2004**, *99*, 210−220.
(56) Jiang, W. Applications of a Configuration-Driven Unitary Group Approach to Electronic Structure Theory. *Ph.D. Dissertation*, University of North Dakota, Grand Forks, ND, 2009.
(57) Peterson, K. A.; Figgen, D.; Dolg, M.; Stoll, H. Energy-Consistent Relativistic Pseudopotentials and Correlation Consistent Basis Sets for the 4*d* Elements Y−Pd. *J. Chem. Phys.* **2007**, *126*, 124101/1−12.
(58) Pou-Amerigo, R.; Merchan, M.; Nebot-Gil, I.; Widmark, P. O.; Roos, B. O. Density Matrix Averaged Atomic Natural Orbital (ANO) Basis Sets for Correlated Molecular Wave Functions III. First Row Transition Metal Atoms. *Theor. Chim. Acta* **1995**, *92*, 149−181.
(59) Baumann, C. A.; Van Zee, R. J.; Bhat, S. V.; Weltner, W., Jr. ESR of Mn_2 and Mn_5 Molecules in Rare Gas Matrices. *J. Chem. Phys.* **1983**, *78*, 190−199.

(60) Haslett, T. L.; Moskovits, M.; Weitzman, A. L. Dissociation Energies of Transition Metal Diatomics. *J. Mol. Spectrosc.* **1989**, *135*, 259−269.
(61) Kirkwood, A. D.; Bier, K. D.; Thompson, J. K.; Haslett, T. L.; Huber, A. S.; Moskovits, M. Ultraviolet-Visible and Raman Spectroscopy of Diatomic Manganese Isolated in Rare-Gas Matrices. *J. Phys. Chem.* **1991**, *95*, 2644−2652.